Quaternary Geochronology 67 (2022) 101242

Contents lists available at ScienceDirect

Quaternary Geochronology

journal homepage: www.elsevier.com/locate/quageo

Characterization of organic matter in marine sediments to estimate age offset of bulk radiocarbon dating

Katrine Elnegaard Hansen [a,*], Jacques Giraudeau [b], Audrey Limoges [c], Guillaume Massé [d], Arka Rudra [e], Lukas Wacker [f], Hamed Sanei [e], Christof Pearce [a], Marit-Solveig Seidenkrantz [a]

[a] Department of Geoscience, Arctic Research Centre and iClimate, Aarhus University, 8000, Aarhus, Denmark
[b] Université de Bordeaux, CNRS, UMR 5805 EPOC, Pessac, France
[c] Department of Earth Sciences, University of New Brunswick, Fredericton, Canada
[d] Université Laval, CNRS, UMI 3376, TAKUVIK, Québec, QC, Canada
[e] Lithospheric Organic Carbon (LOC) Group, Department of Geoscience, Aarhus University, 8000, Aarhus, Denmark
[f] Laboratory of Ion Beam Physics, ETH, CH, 8093, Zürich, Switzerland

ARTICLE INFO

Keywords:
Radiocarbon dating
Organic pyrolysis
Holocene
Marine sediments
Age offset
Bulk organic matter

ABSTRACT

Radiocarbon dating of Arctic marine sediment is often challenging due to the low availability of calcareous fossils. Consequently, bulk organic matter dating has at times been used to establish sediment core chronologies. Yet, radiocarbon dates based on bulk organic matter often appear to deviate vastly from dates based on fossils, mainly caused by input of allochthounous carbon, including terrigenous organic matter. In this study, we aim to examine the link between the composition of the bulk organic matter and the age offsets between the bulk radiocarbon dates and those obtained from calcareous foraminiferal tests. All samples are taken from the marine sediment core AMD14-204C from offshore Upernavik (eastern Baffin Bay). The radiocarbon dates for bulk organic matter are on average ~3000 years older than the radiocarbon dates based on foraminifera, but with changing age offsets throughout the record. To investigate the cause of this age offset and its variations over time, we applied core scanning, X-ray Fluorescence analysis, stable isotopes, organic pyrolysis and microscopic organic petrology to examine the distribution and characterization of the organic matter. The results show that the older organic matter includes clastic input of reworked sedimentary rocks potentially originating from West Greenland and/or the Canadian Arctic Archipelago. Changes in the input of contemporary marine algal produced organic matter versus both terrigenous input and reworked ancient organic matter appear to control the age offsets between the bulk and foraminifera dates. A low Hydrogen Index and low $\delta^{13}C_{org}$ values together with a high Oxygen Index, indicative of high influence of terrigenous organic matter, seem to correspond to samples with the largest age offsets; 1000–2000 years greater than in other samples. To examine the cause of the variations in the age offsets, a new quantification of the autochthonous organic matter as a fraction of the TOC was calculated. This shows that samples with the largest age offsets contained the lowest fraction (as low as ~12%) of autochthonous organic matter in the TOC.

1. Introduction

In paleoceanographic and paleoclimatic reconstructions based on marine sediment cores, precise age controls of the sediments are imperative to establish firm time constraints of the climatic and oceanographic changes. These are necessary both for estimating rates of local change and for comparing climate developments over a large geographical area. However, constructing an age model based on radiocarbon dates for marine sediment cores in the Arctic marine realm is often challenging since the amount of carbonate macrofossils and microfossils is limited. For that reason, bulk sediment samples containing minerogenic material and organic matter of different origins have been used for dating and establishing age-depth models (Andrews et al., 1985; Fillon et al., 1981; Giraudeau et al., 2020; Licht et al., 1998; Muschitiello et al., 2020). However, the introduction of allochthonous organic matter to the study site will affect the reliability of the radiocarbon dates on bulk sediments. Thus, when radiocarbon dating is performed on both bulk sediment samples and fossils, the latter having a

* Corresponding author.
E-mail address: katrine.elnegaard@geo.au.dk (K.E. Hansen).

https://doi.org/10.1016/j.quageo.2021.101242
Received 4 November 2020; Received in revised form 24 September 2021; Accepted 14 October 2021
Available online 16 October 2021

much lower risk of contamination by older organic material when properly cleaned, the two sets of dates may have distinct offsets in the same record.

To characterize and determine the source and relative contribution of marine and terrigenous organic matter in the Arctic region, organic pyrolysis and organic petrography have previously been applied on surface sediment samples (Boucsein et al., 2002; Boucsein and Stein, 2000; Fahl & Stein, 1997, 1999; Wagner and Henrich, 1994). Pyrolysis geochemistry and organic petrography are methods most commonly used in geological oil exploration, to determine the thermal maturity of source rocks. However, the aforementioned studies based on surface sediment samples demonstrated that the Hydrogen Index (HI), informs on variations between terrigenous and marine sources of the organic matter, with high HI values being closely related to large amounts of fresh autochthonous algal rich marine organic matter (Boucsein et al., 2002; Boucsein and Stein, 2000; Fahl & Stein, 1997, 1999; Wagner and Henrich, 1994). By contrast, a high Oxygen Index (OI), which represents the amount of oxygen relative to organic carbon, is considered indicative of elevated influence of terrigenous organic matter (Carrie et al., 2012; Fahl and Stein, 1999; Lafargue et al., 1998).

Our aim is to use organic pyrolysis combined with organic petrography to evaluate the source of organic material in a marine sediment record, and in particular, to explain changes in bulk date age offsets. Hence, we use organic petrography and Rock-Eval® organic pyrolysis to determine the different types and the source of the organic matter in the marine sediment core. This is done by examining variations in the non-generative ^{14}C-depleted organic components, the Total Organic Carbon (TOC), HI and OI. We also compare the organic pyrolysis parameters and organic petrography results with X-ray Fluorescence core scan data and the stable isotope ratio $\delta^{13}C_{org}$. The study is based on the analysis of a 738 cm long marine sediment core, AMD14-204C, retrieved from 987 m water depth in the eastern Baffin Bay near the Upernavik Isstrøm (73°15.663′ N, 57°53.987′ W) (Fig. 1). ^{14}C measurements have been performed both on bulk organic matter (Giraudeau et al., 2020) and on benthic and planktonic foraminifera (Hansen et al., 2020), making it possible to investigate potential age offsets and their link to organic matter composition.

2. Study area

The Baffin Bay is a semi-enclosed basin constrained by the Canadian Arctic islands (e.g., Ellesmere Island and Baffin Island) to the west and northwest and Greenland to the east. The Baffin Bay receives water mass contributions from the south via the Labrador Sea and from the north via the Arctic Ocean. The water masses penetrating from the south are relatively warm and conveyed by the West Greenland Current (WGC) containing both colder water masses from the East Greenland Current (EGC) and warmer saline waters from the Atlantic Irminger Current (IC) (Drinkwater, 1996; Münchow et al., 2015; Tang et al., 2004). From the north-northwest cold low saline surface waters are delivered to the Baffin Bay via the Canadian Arctic Archipelago gateways; Lancaster Sound, Jones Sound and Nares Strait, flowing southward (Drinkwater, 1996), where parts of the cold surface water masses recirculates eastward towards the eastern part of the Baffin Bay. Additionally, cold and saline bottom waters fill the deeper parts of the Baffin Bay (1200–1800 m water depth) (Tang et al., 2004).

The exposed bedrock surrounding the northeastern and northwestern Baffin Bay is mainly composed of different types of gneisses, granites and sedimentary rocks (Harrison et al., 2011) (Fig. 1a). The geology of Ellesmere Island is dominated by Palaeozoic limestone deposits, together with minor outcrops of Mesozoic sediments. A continuation of the limestones is observed in the northernmost part of Greenland, with little to no limestone along the northwest coast of Greenland. This part of Greenland is dominated by different gneisses, granites, basalts and marbles, where the few sediment outcrops along western Greenland are located in the Disko Bugt area. Here the sediment

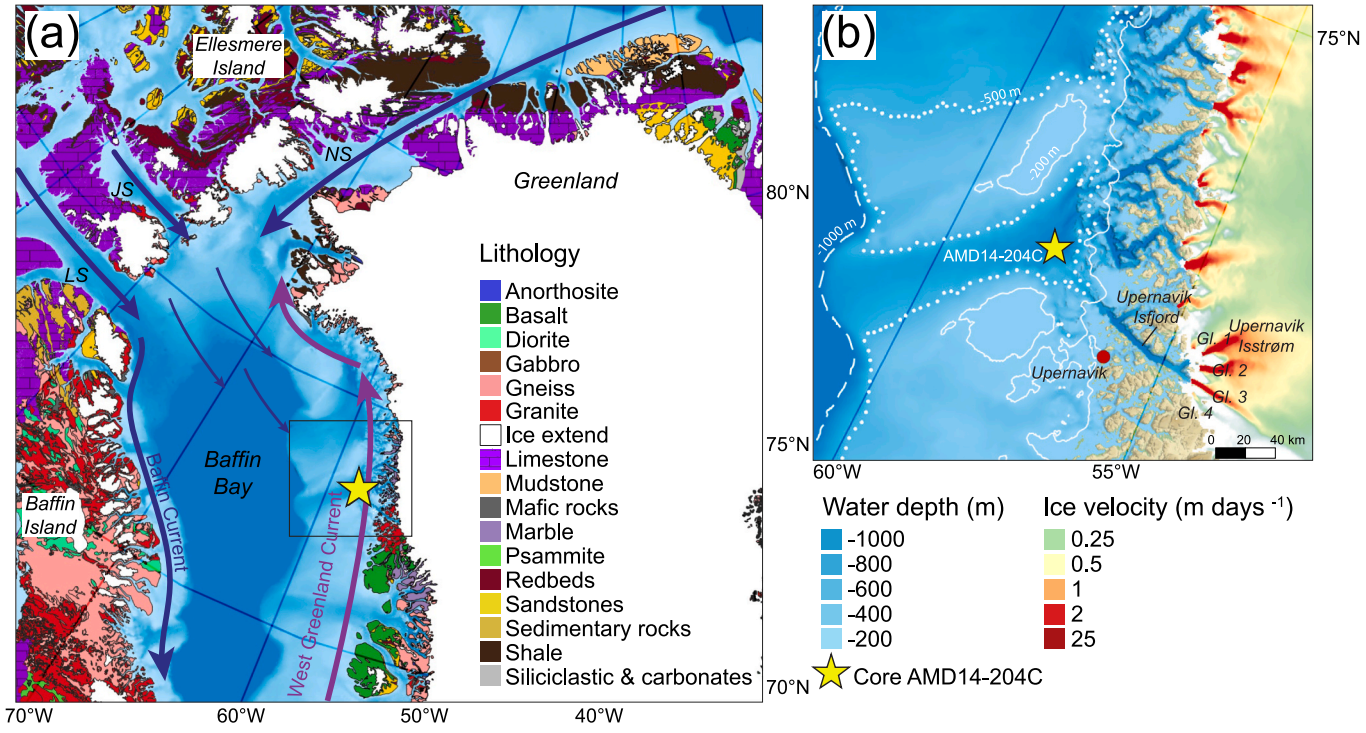

Fig. 1. (a): An overview of the geology of Baffin Island, Ellesmere Island and northwestern Greenland, modified after Harrison et al. (2011), together with modern ocean surface currents and study site. Purple and blue arrows indicate intermediate and cold water temperatures, respectively. LS = Lancaster Sound, JS = Jones Sound, NS = Nares Strait. (b) Zoom in on area defined by the black box in panel (a), showing the Upernavik Isfjord and Isstrøm, comprising four glaciers. Ice velocity data is derived from Sentinel-1 SAR data acquired from 2017 to 12-28 to 2018-02-28 (Nagler et al., 2015). Ocean bathymetry and bed topography data is derived from GEBCO and BedMachine v3 (Morlighem et al., 2017; Weatherall et al., 2015).

outcrops consist mainly of Cretaceous marine clay stones, locally sandy/silty (Dam et al., 1998; Gregersen et al., 2020). The eastern Baffin Island is largely composed of some limestones towards the north but it is otherwise largely dominated by gneisses and granites. The Upernavik Isstrøm is located adjacent to the core site (Fig. 1b) and is primarily surrounded by Precambrian charnockite and orthopyroxene granite (Escher and Pulvertaft, 1995; Harrison et al., 2011). The four glaciers that make up this ice stream are fast flowing and drain approximately 65 000 km^2 of the Greenland Ice Sheet (Haubner et al., 2018; Vermassen et al., 2019a), plausibly leading to surrounding local bedrock injections to the Upernavik Isfjord and further to the deep sea during periods of increased glacial drainage (Vermassen et al., 2019b; Giraudeau et al., 2020).

3. Background data

3.1. Chronology

The fossil-based age-depth model of the marine sediment core AMD14-204C has previously been presented by Hansen et al. (2020) and was based on AMS ^{14}C dating of 11 intervals. The dated material consisted mainly of benthic foraminifera, but planktonic foraminifera and ostracods were also included in some samples due to the scarcity of calcareous benthic foraminifera (Table 1). The conventional radiocarbon ages for these intervals were calibrated with the software OxCal v4.3 (Ramsey, 2008), applying the Marine13 calibration data (Reimer et al., 2013), and a marine reservoir correction of $\Delta R = 140 \pm 30$, which has previously been used in this region (e.g. Jackson et al., 2017; Lloyd et al., 2011; Perner et al., 2012). The dates obtained on benthic vs. planktonic foraminifera from the same level were comparable (Hansen et al., 2020), suggesting a similar reservoir age for the two foraminiferal groups. However, only the dates on the benthic foraminifera were included in the age model. A depositional *P_sequence* model was applied on the radiocarbon ages of the 11 intervals with a k-value of 0.68 for the age-depth model (Ramsey, 2008). The 11 AMS dates on mainly benthic foraminifera are used in the age-depth model to obtain the modelled median ages (Table 1).

Additionally, the bulk organic matter of 10 intervals were radiocarbon dated (Table 1); these have previously been included in an age model for core AMD14-204C presented by Giraudeau et al. (2020). Pre-treatment and radiocarbon dating of these samples were carried out at the Beta Analytic testing laboratory. The first step of the pre-treatment procedure involved dispersion of the sediment with the purpose of increasing the sediment surface as much as possible. This procedure was followed by repeated application of HCl (acid wash) to ensure the absence of carbonates (Beta Analytic Standard Pretreatment Protocols). The radiocarbon dates based on bulk organic matter were calibrated using the same procedure as for the radiocarbon dates based on benthic foraminifera and with the same ΔR value of 140 ± 30 years for the Marine13 calibration curve (Reimer et al., 2013), in accordance with the $\delta^{13}C_{org}$ data, which despite some terrestrial influx indicate dominance of organic matter of marine origin in much of the core (Table 1).

The results of the foraminiferal-based age-depth model are presented in Fig. 2a, together with the 10 radiocarbon dates performed on bulk organic matter. For both bulk and foraminiferal dates, we here keep the original age models as published by Giraudeau et al. (2020) and Hansen et al. (2020) as it allows a direct comparison with all previously published data from this core. The age model based on datings of foraminifera reveals that the sediment core spans over the last 9200 cal years BP (Hansen et al., 2020). The age offset between the two types of radiocarbon dates is calculated as the difference (in yrs) between the median calibrated age of the bulk samples and the corresponding

Table 1
List of radiocarbon dates and modelled ages from core AMD14-204C. All dates were calibrated using the Marine13 calibration curve (Reimer et al., 2013) and $\Delta R = 140 \pm 30$ years. Median ages marked with * are included in the age-depth model.

Depth midpoint (cm)	Lab. ID	Material	^{14}C age (yr BP)	Calibrated age range (cal yr. BP), 1σ	Median age (cal. yr BP)	$\delta^{13}C_{org}$ (‰)
4.5	ETH-92277	Mixed benthic foraminifera	705 ± 50	167–276	*213	–
29.5	BETA 480648	Organic matter	3290 ± 30	2838–2957	2897	−21.6
70.5	ETH-92279	Mixed benthic foraminifera	1795 ± 50	1175–1270	*1216	–
75.5	BETA 480647	Organic matter	3780 ± 30	3452–3561	3509	−21.8
125.5	BETA 480646	Organic matter	4640 ± 30	4600–4770	4666	−21.8
157.5	BETA 480645	Organic matter	5650 ± 30	5820–5923	5869	−21.8
170	SacA 46 004	Mixed benthic & planktonic foraminifera	3555 ± 35	3139–3260	*3192	–
237.5	BETA 480644	Organic matter	6410 ± 30	6638–6793	6691	−21.8
250.5	BETA 467785	Mixed benthic & planktonic foraminifera	4300 ± 30	4133–4254	*4199	–
310.5	ETH-92281	Mixed benthic foraminifera	4950 ± 60	4860–4992	*4941	–
329.5	BETA 480643	Organic matter	7820 ± 30	8053–8163	8109	−21.9
410.5	ETH-92283	Mixed benthic foraminifera	5805 ± 60	5905–6005	*5959	–
491.5	BETA 480642	Organic matter	8960 ± 30	9430–9498	9462	−22.5
501.5	BETA 488641	Mixed benthic foraminifera	6400 ± 30	6656–6751	*6707	–
580.5	ETH-92285	Mixed benthic foraminifera	7155 ± 70	7430–7531	*7483	–
610	SacA 46 005	Mixed benthic foraminifera & ostracods	7445 ± 50	7712–7822	*7766	–
614	BETA 480641	Organic matter	10670 ± 30	11579–11876	11711	−22.9
683.5	BETA 480640	Organic matter	11170 ± 30	12524–12612	12566	−22.8
700.5	ETH-92286	Mixed benthic foraminifera	8270 ± 390	8639–8885	*8755	–
713.5	BETA 480639	Organic matter	11710 ± 30	12951–13103	13024	−22.8
737.5	ETH-92287	Mixed benthic foraminifera	8490 ± 150	9017–9302	*9162	–

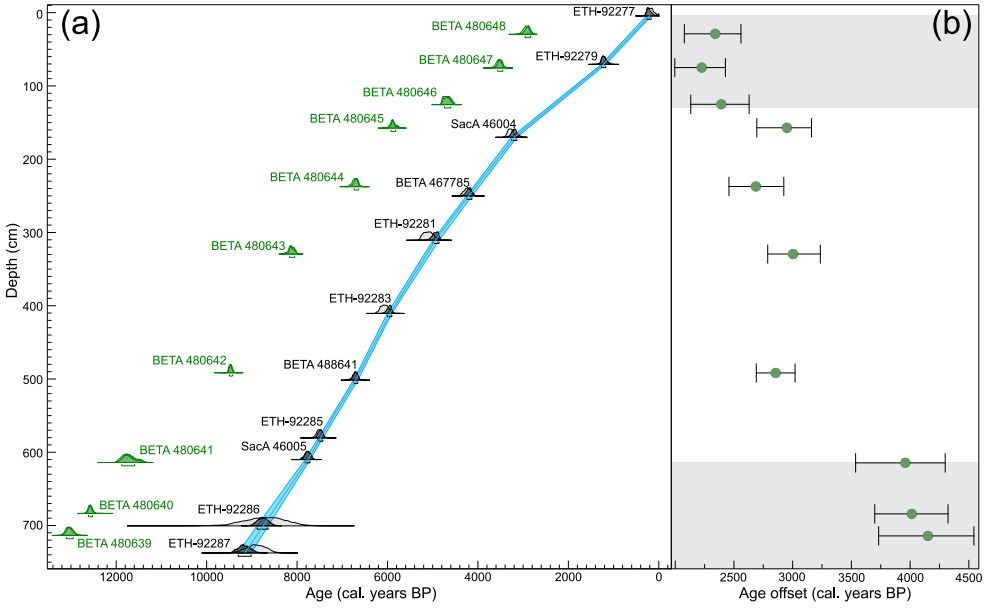

Fig. 2. (a) Age-depth model of the marine sediment core AMD14-204C, based on mainly mixed benthic foraminifera (grey age distributions; the light shaded area for each radiocarbon date illustrate the probability distribution before age modelling, while the darker grey areas represent the probability distribution after age modelling. The modelled age is shown in blue, with the envelope representing the modelled 1σ range) (Hansen et al., 2020). The bulk organic matter dates are plotted in green (Giraudeau et al., 2020). (b) Age offsets between median calibrated bulk dates and the corresponding modelled age for each depth interval with 2σ uncertainties, calculated based on the 2σ age ranges derived from the age modelling. The grey and white boxes illustrate the three-part division of the record.

modelled median age for the same depth level based on the foraminifera-based age-depth model, see Figs. 2b and 3.

The age offset varies between c. 2225 and 4150 cal years BP for the entire core, and may be divided into three different zones in the core (Fig. 2b). The largest age differences are observed in the bottommost part of the core (738–614 cm) reaching c. 4000 cal years BP on average. The age offset decreases abruptly above 614 cm core depth, reaching an average value of 2875 cal years BP from c. 490 cm to c. 130 cm core depth. The top most part of the core exhibits the lowest age differences of approximately 2300 cal years BP.

3.2. X-ray fluorescence

XRF data (Fig. 4) are often used in paleoenvironmental studies to evaluate changes in the relative contribution of marine and terrigenous sediments (Jansen et al., 1998; Ren et al., 2009; Seidenkrantz et al., 2007). The XRF scan was conducted on core AMD14-204C in increments of 5 mm using an AVAATECH scanner at the EPOC laboratory in Bordeaux, France, logging the geochemical elemental composition of the core with minimum sediment disturbance. The generator settings of 10, 30 and 50 kV with a Rhodium (Rh) tube was applied to obtain the full elemental spectra from Al to Ba. For further information on the composition of this dataset see Giraudeau et al. (2020) and Hansen et al. (2020).

In this study, we consider potassium (K) and rubidium (Rb) as indicators of increased terrigenous runoff, based on the elemental composition of the bedrock near the core site (Saito, 1998; Steenfelt, 2001; Steenfelt et al., 1998), and bromine (Br) as an indicator for autochthonous marine organic matter originating from marine biological productivity (Pruysers et al., 1991). Thus, the Rb/Br ratio was calculated to assess the relative changes in down-core terrigenous influence (Fig. 4). The element K and the ratio Rb/Br appear to co-vary throughout most of the core. From the bottom of the core up to ~614 cm, the elemental composition of the sediment contains relatively higher counts of K and Rb/Br. This interval is followed by a sudden decrease in Rb/Br and K. The elements do not appear to vary significantly after 614 cm core depth, except for a gradually decreasing trend in Rb/Br and K towards the core top.

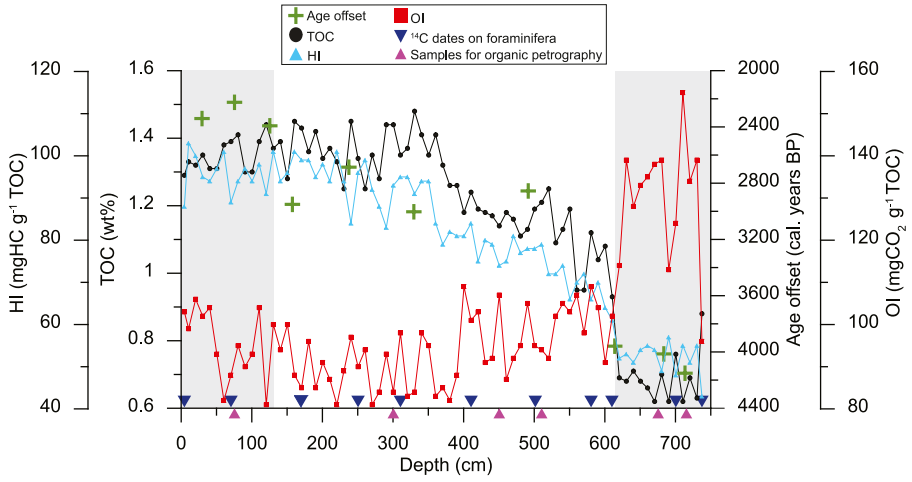

Fig. 3. Hydrogen Index (HI), TOC, age offset between bulk organic matter ^{14}C dates and the age model based on ^{14}C dates of mainly benthic foraminifera, intervals sampled for organic petrography and Oxygen Index (OI) plotted against core depth of the marine sediment core AMD14-204C. The grey and white boxes illustrate the three-part division of the record.

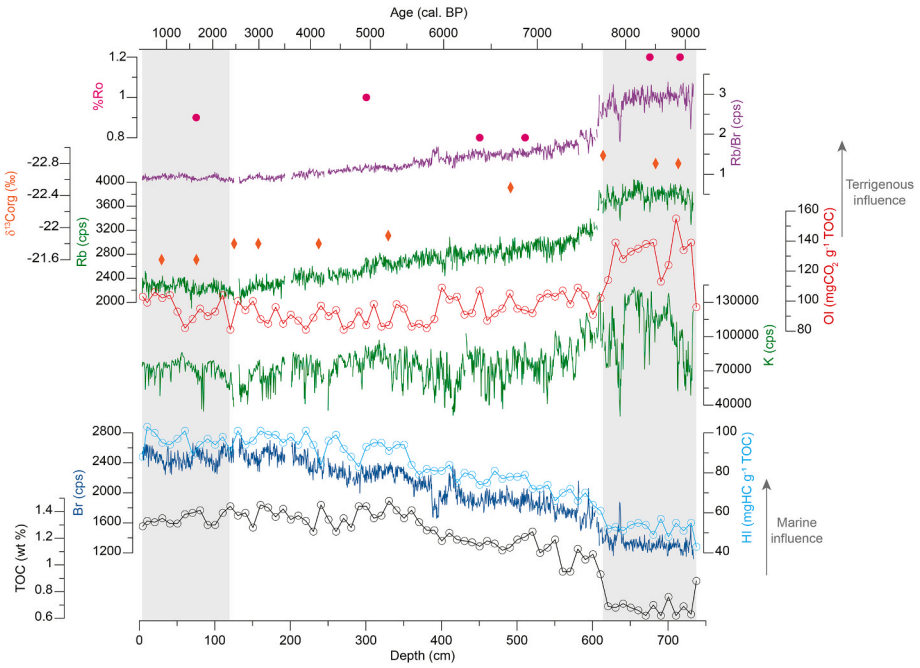

Fig. 4. Comparison of organic pyrolysis parameters, the median %Ro, organic $\delta^{13}C$ and X-ray Fluorescence data of core AMD14-204C. The grey and white boxes illustrate the three-part division of the record.

3.3. Stable isotopes

The stable carbon isotopic ratio $\delta^{13}C_{org}$ (Fig. 4) has been applied in marine and lacustrine studies to determine the relative contribution of marine and terrigenous organic matter in sediments. Sediment with high marine algal contributions has $\delta^{13}C_{org}$ values ranging from around −22‰ to −17‰ (Descolas-Gros and Fontugne, 1985; Meyers, 1994), whereas values for terrigenous-influenced sediment range between −30‰ and −22‰ (Arthur et al., 1983; Meyers, 1994). The ratio of the stable carbon isotopes, $\delta^{13}C_{org}$, was measured on the bulk organic matter samples in connection with the radiocarbon dating. The $\delta^{13}C_{org}$ was measured using an isotope-ratio mass spectrometer (IRMS) at the Beta Analytics Stable Isotope laboratory, and all reported values are relative to the VPDB-1. In our study, the measured $\delta^{13}C_{org}$ varies between −22.9‰ and −21.6‰ (Fig. 4). The lowest values are found in the bottommost part of the core between 738 and 614 cm. The values for the rest of the core varies little (−21.9‰ to −21.6‰) except for one low measurement of −22.5‰ at 490 cm.

4. Methods

4.1. Pyrolysis geochemistry of organic matter

Subsampling for the pyrolysis was carried out at Aarhus University at every 10 cm for the entire core. Approximately 100–150 mg of wet bulk sediment was subsampled into glass vials covered with aluminum foil with one side open to allow for evaporation of water. The wet bulk samples were then dried at 30 °C in an oven, before they were crushed into fine powder of which approximately 50 mg were put into metal vials. The metal vials were then loaded into a HAWK Pyrolysis and TOC Instrument, Wildcat Technologies of the Lithospheric Organic Carbon (LOC) laboratory of Aarhus University.

The Rock-Eval® method was applied in order to measure the different types of organic matter in bulk sediment samples (Carrie et al., 2012; Lafargue et al., 1998; Sanei et al., 2000, 2001). The method consist of a two-step procedure, where the pyrolysis step takes place in an inert helium atmosphere and the combustion occurs in an oxic atmosphere. During the pyrolysis, the samples were subjected to 300 °C for 3 min. This releases the free protohydrocarbons being the most readily degradable, volatile, preserved labile organic matter denoted the S1 fraction (mg hydrocarbon/g sediment). The samples were subsequently subjected to a temperature ramp of 25 °C per minute until a temperature of 650 °C was reached, to release the hydrocarbons in the S2 fraction (mgHC/g sediment), which is composed of more stable and higher molecular weight hydrocarbons derived mainly from autochthonous algal matter. Thus, organic matter in the S2 fraction consist of algal biomacromolecular structures (Carrie et al., 2012; Outridge et al., 2007; Sanei and Goodarzi, 2006). S2 is measured with an accuracy and precision of better than 4%. The amount of CO_2 and CO from the breaking of carboxyl groups and other oxygen containing organic matter are represented by the $S3CO_2$ (mg CO_2/g sediment) and S3CO (mg CO/g sediment) fractions, respectively and these fractions are measured continuously during the pyrolysis with an accuracy of 10% and 3%, respectively. S3 is composed of humic organic matter and terrigenous plant matter (cellulosic/lignin) (Carrie et al., 2012; Lafargue et al., 1998). In the next step, the sample is oxidized up to 850 °C, incinerating all the remaining organic matter and producing the residual carbon fraction (RC, wt.%), including the S4 fractions (Lafargue et al., 1998).

The TOC is derived from the sum of the reactive, pyrolysable organic carbon (PC, wt.%) and residual organic carbon (RC, wt%):

$$TOC(wt\,\%) = PC\ (wt\,\%) + RC\ (wt\,\%)$$

where RC (wt%) is the organic carbon derived from: $S4CO_2$+S4CO. PC (wt%) is the organic carbon derived from: S0+S1+S2+$S3CO_2$+S3CO+($S3'CO_2$) (Lafargue et al., 1998). The TOC is measured with an accuracy and precision of better than 2%.

The Hydrogen Index (mgHC g^{-1} TOC) is derived from the following equation (Lafargue et al., 1998):

$$HI = \frac{S2}{TOC} * 100$$

It is a measure of hydrogen-rich compounds and the relative freshness/immaturity of the organic matter (Carrie et al., 2012; Fahl and Stein, 1999). Studies on recent marine sediment cores reveal that higher HI-values are linked to marine conditions associated with marine algal productivity with little to no introduction of terrigenous sediments

(Boucsein et al., 2002; Boucsein and Stein, 2000; Carrie et al., 2012; Fahl & Stein, 1997, 1999; Wagner and Henrich, 1994).

The Oxygen Index (OI; $mgCO_2\ g^{-1}$ TOC) is the $S3CO_2$ normalized to TOC. It is related to the amount of oxygen in the organic matter and is derived from the following equation (Lafargue et al., 1998):

$$OI = \frac{S3CO_2}{TOC} * 100$$

It indicates how terrigenous in origin the organic matter is (Fahl and Stein, 1999; Lafargue et al., 1998). However, a study on soil organic matter shows that lipids degrade first, derived from a decrease in HI values down core concurrent with increasing OI values (Disnar et al., 2003). Thus, this can also be interpreted as selective preservation of compounds or a change in the organic matter source. However, environmental interpretations of both OI and HI need to be supported by organic petrography analysis.

4.2. Organic petrography

Organic petrography microscopy analyses were performed on selected samples in order to support the pyrolysis data by making both a qualitative and quantitative study of organic matter.

Samples for organic petrography were collected at depth midpoints 75.5 cm, 300.5 cm, 450.5 cm 510.5 cm, 675.5 cm and 715.5 cm (Table 2). The samples were retrieved from core intervals with varying TOC, identified through the pyrolysis. From all sample depths approximately 4 cc of wet sediment was retrieved and placed into glass vials and freeze-dried. When completely dry the samples were mixed with an epoxy-resin mixture in a mould. After drying, the samples were successively sanded with P200 and P100 sandpapers. Finally, the samples were polished with a 1 μm polishing pad. Diamond spray was applied in all sanding and polishing processes.

For the organic petrography analysis, an incident-light, white and fluorescence microscopic system (Zeiss AxioImage MII) equipped with a Discus-Fossil system was used at the Lithospheric Organic Carbon (LOC) Laboratory of Aarhus University. The reflectance (% Ro) of 50 randomly orientated vitrinite and inertinite macerals (allochthonous, land-derived organic fragments derived from geological sedimentary rocks) was measured under oil immersion (objective × 50) to evaluate the different organic carbon sediment sources. The number of vitrinites and inertinites was also counted while scanning through the samples until 50 measurements for each sample were obtained. The %Ro measurements were typically conducted on fragments ranging from ~2 to ~12 μm. The vitrinite macerals larger than 10 μm in diameter were measured twice, since they represent a larger volume distribution in the sediment. A quantification of the macerals was not possible due to their low concentration.

The samples were also subjected to fluorescence microscopy to determine the degree of degradation and the general composition of the samples. By exposing chlorophyll and labile organic matter to a strong ultra violet light source, instant degradation of this material occurs, by visualized fading of fluorescence intensity of the chlorophyll and labile organic matter.

Table 2
Overview of the samples taken for organic petrography, the median %Ro for each sample and the relative distributions of the organic macerals.

Depth (cm)	Median % Ro	Group A		Group B		Group C	
		%	Mean % Ro	%	Mean % Ro	%	Mean % Ro
75–76 cm	0.9	64	0.7	34	1.6	2	2.7
300–301 cm	1.0	56	0.7	44	1.6	0	–
450–451 cm	0.8	70	0.7	24	1.6	6	2.5
510–511 cm	0.8	84	0.7	12	1.6	4	2.4
675–676 cm	1.2	46	0.8	50	1.5	4	2.5
715–716 cm	1.2	41	0.7	47	1.6	10	2.6

5. Results

5.1. Organic pyrolysis geochemistry

The results of the organic pyrolysis analysis are shown in Figs. 3 and 4. These results indicate that TOC and HI co-vary down-core, where the lowest values are recorded at 738-614 cm core depth (~0.6% TOC and HI: ~52 $mgHC\ g^{-1}$ TOC). In addition, the OI shows an opposite pattern to TOC and HI, and exhibits the highest values at this core interval (OI: ~130 $mgCO_2\ g^{-1}$ TOC). From 614 cm to around 510 cm, the OI shows a pronounced decrease (OI: ~100 $mgCO_2\ g^{-1}$ TOC) concurrent to an increase in HI and TOC (HI: ~70 $mgHC\ g^{-1}$ TOC, TOC: 1.1%). The TOC decreases slightly after 510 cm followed by a steady increase until 360 cm core depth. Contemporarily, the OI shows intermediate and fluctuating values. HI and TOC record the highest values from 360 cm to 130 cm (TOC: ~1.4%, HI: ~94 $mgHC\ g^{-1}$ TOC) whereas the OI is low (~90 $mgCO_2\ g^{-1}$ TOC). OI and HI do not vary vastly from 130 cm towards the core top, whereas a minor decrease is observed in TOC.

5.2. Organic petrography

Organic petrography reveals the distribution of allochthonous, ^{14}C-depleted clastic organic fragments (macerals). Macerals are categorized into vitrinites and inertinites. Vitrinites are common constituents of carbonaceous sedimentary rocks, originating from the cellulosic and lignin-based, terrigenous organic carbon at the geological time of deposition, whereas inertinites, represent highly refractory organic macerals derived mainly from either geological or recent thermal degradations (Bustin et al., 1985; van Krevelen, 1993; Stach et al., 1982). The reflectance measurements were conducted on vitrinite and inertinite macerals (Fig. S4; supplementary material). Vitrinite fragments commonly show lower reflectance (%Ro) values than inertinite.

We defined three maceral groups based on the different %Ro distributions in our samples. The vitrinite macerals are generally represented by two distinct reflectance populations (groups A and B) based on the bimodal distributions of the vitrinite reflectance values (%Ro) in the frequency distribution histograms (Law, 1999) (Fig. 5). Group A includes vitrinites with reflectance values below 1.1% (mean %Ro value of 0.7% for all samples combined). Group B is defined as vitrinites with % Ro between 1.1% and 2.3% and shows a mean %Ro of 1.6% for all the samples combined. Group C encompasses the organic components with the highest reflectance values of more than 2.3%, corresponding to the oxidized macerals inertinites, based on both these distinctly high %Ro and visual characteristics of the macerals. The mean %Ro for group C is 2.5%. The median %Ro for each sample is also shown in Table 2 and plotted as pink dots in Fig. 4.

Most vitrinite samples in group A have an unimodal distribution, whereas an unimodal distribution in group B is only observed in some of the samples (Fig. 5). Additionally, the mean %Ro values for the groups in each sample do not differ much from the mean %Ro for the combined measurements of all samples. However, the two bottom most samples at 715-716 and 675–676 cm core depth, are distinct in having a higher median %Ro, the largest B groups and smallest A groups compared to the other samples. The bimodal distribution of groups A and B are not clear at a depth of 715–716 cm, but easily recognizable at a depth of 675–676 cm. One relatively high measurement in sample 715–716 cm of 3.1 %Ro was potentially minerogenic and not organic and therefore omitted from group C.

The samples at 510–511 cm and 450–451 cm both have a lower median %Ro than the two bottom samples. Also, in contrast to the two lowermost samples, group B is also much smaller than group A and the

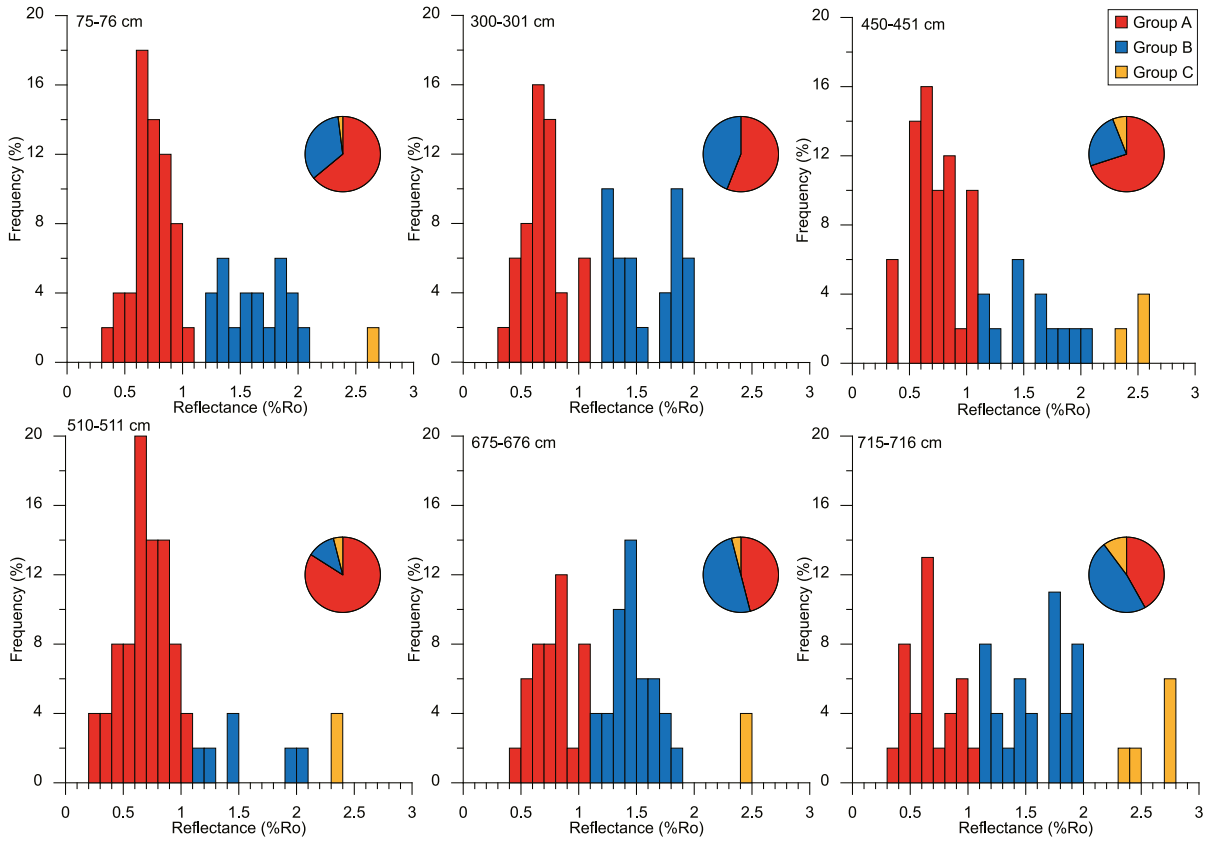

Fig. 5. The distributions and percentage frequencies of the counted organic vitrinites (groups A and B) and inertinites (group C) in the samples from various depths shown both as histograms and pie charts.

bimodal structure is less prominent to near absent at 510-511 and 450–451 cm. At 510–511 cm group A consists of 84% of the macerals, whereas group B only constitutes 12% of the macerals. Like in the samples below (675–676 cm and 715–716 cm), only a few macerals belong to group C.

The vitrinites in the two topmost samples at 75–76 cm and 300–301 cm show a distinct bimodal distribution, with groups A and B being much closer in size. In contrast group C is near absent. The median %Ro appears to increase slightly towards the core top.

6. Discussion

The relative variations in the measured pyrolysis parameters, elemental composition (XRF) and stable isotopes suggest that the type and source of organic matter have changed throughout the core affecting the age offset between radiocarbon dates based on foraminifera and those based on bulk organic matter. High HI, $\delta^{13}C_{org}$ and Br at the uppermost part of the core document high autochthonous organic matter input (in this case, derived from marine algal productivity) (Boucsein et al., 2002; Carrie et al., 2012; Fahl & Stein, 1997, 1999; Wagner and Henrich, 1994; Pruysers et al., 1991; Descolas-Gros and Fontugne, 1985; Meyers, 1994; Sanei et al., 2000, 2001). In contrast, core intervals with high OI, Rb and K together with low $\delta^{13}C_{org}$ indicate that the sediment and organic matter carry a strong terrigenous signal (Carrie et al., 2012; Fahl and Stein, 1999; Lafargue et al., 1998). Based on our results we define three quantifiable main sources of organic matter present in the marine sediment core; 1) contemporary autochthonous marine algal organic matter derived by the HI, 2) terrigenous organic matter derived by the OI and 3) other reworked allochthonous organic matter. Comparing these parameters with the organic petrography results can aid the investigation of down core changes in sediment and organic matter sources.

The organic petrography analyses document the presence of vitrinites and inertinites, which are terrestrially-derived organic components (macerals) with distinct chemical compositions (Bustin et al., 1985; Stach et al., 1982); they make up the non-generative part of the TOC and are thus depleted in ^{14}C. When organic carbon from plant tissue is incorporated in sediments and is deeply buried, it becomes heated and the reflective properties change, fostered by increasing condensation of aromatic structures in the macromolecules. Inertinites are more refractory than vitrinites and thus have higher reflectance values representing higher degree of oxidation and alterations (Bustin et al., 1985; van Krevelen, 1993; Stach et al., 1982). Consequently, the reflectivity of the maceral fragments are used to record the maximum burial heating of a sample (vitrinite reflectance or %Ro).

The %Ro values can be used to trace the source of the sediments, based on the regional burial of their precursor sedimentary rocks. When comparing our reflectance analysis results to existing data on regional thermal maturity (reflectance of macerals) of carbonaceous sedimentary outcrops of the Baffin Bay region, we may thereby deduct their most likely sources. The vitrinites in group A (mean %Ro = 0.7%) have similar %Ro values to the Cretaceous sedimentary rocks found in Disko Bugt (West Greenland) and the Canadian Arctic Archipelago (Dam et al., 1998; Dewing et al., 2007; Gentzis and Goodarzi, 1991; Mukhopadhyay et al., 1997). Group B with its higher mean %Ro of 1.6% is indicative of more thermally mature sedimentary rocks. The Northeastern Canadian Arctic islands have vast outcrops of Paleozoic sedimentary rocks, with mean %Ro close to that of the group B vitrinites in our samples (Harrison et al., 2008). The inertinites in group C are potentially sourced from West Greenland sediments that have been thermally altered by Paleogene volcanism and yielding high Ro% matching those found in group C (Abdelmalak and Polteau, 2020; Green, 2003; Japsen et al., 2005).

However, windblown charred wood or coal from forest fires exhibits the same high reflectance values and could potentially also be the source of the group C inertinite fragments (Scott and Glasspool, 2007).

Vitrinites and inertinites are reworked from the terrigenous sedimentary outcrops, redistributed and deposited in the marine realm by ocean currents or wind. Most of the vitrinites and inertinites present in the samples had a size range of a few microns, whereas only a few of them were larger than 10 μm (See Fig. S1 to S6 in supplementary), indicative of long suspension and transportation potential. However, applying the reflectance analysis as a reliable provenance tool in marine sediment core studies require further investigation, especially since degradations during transport of vitrinites to the marine may, to some degree, increase the reflectance values (Liu et al., 2020). Both vitrinites and inertinites thus represent previously deeply buried organic material, reworked from old sediments.

6.1. Changes in organic source material

6.1.1. 738-614 cm

The bottommost core interval has the highest age offset of the entire core between the bulk organic matter dates and foraminiferal-based dates. This high age offset (ca. 4000 years average) suggests a comparatively higher dominance of older allochthonous organic matter to the core site combined with a more limited production of contemporary marine algal organic matter, as also supported by the low HI and low Br counts (Boucsein et al., 2002; Boucsein and Stein, 2000; Carrie et al., 2012; Fahl & Stein, 1997, 1999; Wagner and Henrich, 1994; Pruysers et al., 1991). The elevated OI, K and Rb values indicate a terrigenous source for this old organic matter (Carrie et al., 2012; Fahl and Stein, 1999; Lafargue et al., 1998; Saito, 1998; Steenfelt, 2001; Steenfelt et al., 1998). This is further supported by the three $\delta^{13}C_{org}$ measurements for this interval that vary between −22.9‰ and −22.8‰ and thus exhibit a mixed marine and terrigenous signature (Arthur et al., 1983; Ehleringer et al., 1997). Based on the interpretations of benthic foraminifera and XRF data in Hansen et al. (2020), this time interval covers the final phase of the deglaciation and thus a period of enhanced meltwater run off from the Greenland Ice Sheet to the West Greenland shelf. The relative increase of reworked organic material was likely incorporated in ground-up glacial drift deposits (Hansen et al., 2020).

The results of the organic petrography show that the two samples from this interval (715–716 cm and 675–676 cm) are distinctively different from the samples above. This is demonstrated by the large group B and small group A, together with the higher median %Ro. The bottom most sample (715–716 cm) does not show a clear bimodal distribution, which could be attributed to increased mixing from deglacial meltwaters. This suggests that the sediment and organic matter source in this interval is characteristically different from the rest of the core. The deposition of allochthonous organic carbon, together with low marine productivity reflected by low HI presumably caused the very high age offset here.

6.1.2. 614-130 cm

At a core depth of ~614 cm, a prominent shift in the elemental composition, pyrolysis parameters and age offset, points to a change in the general sediment and organic matter composition. This shift is associated with an overall decreasing yet fluctuating trend in the age offset throughout this core interval (average age offset of ~2875 cal years BP).

Decreasing values of the terrigenous organic matter indicators OI, K, and the Rb/Br ratio, document a comparatively reduced influence from allochthonous organic matter, presumably facilitated by a reduction in meltwater injections from the Upernavik Isstrøm (Hansen et al., 2020). This coincides with increasing HI and $\delta^{13}C_{org}$, implying enhanced production of autochthonous algal matter, which is also reflected by the lower age offset here (Boucsein et al., 2002; Carrie et al., 2012; Fahl and Stein, 1999; Lafargue et al., 1998; Pruysers et al., 1991; Saito, 1998; Steenfelt, 2001). The presence of diatoms and contemporary marine algal produced organic matter represented by the HI was clearly observed in the organic petrography samples 300–301 cm, 510–511 cm and 450–451 cm, where both large diatoms and light blue patches in the sediment matrix clearly appeared under fluorescence light (see supplementary Figs. S2, S3 and S4). For sample 300–301 cm clear patches of chlorophyll (red areas) appeared and these were not observed in the other samples. These patches of chlorophyll are indicative of very good preservation, presumably facilitated by relatively higher sedimentation rates (Hansen et al., 2020), since the degradation of chlorophyll occurs rapidly if the material is not buried relatively fast. This is demonstrated by exposing the sample to a strong fluorescence source for just a couple of seconds, where the strong red color clearly fades away (see supplementary Figs. S2B and S2C). In addition, the three petrography samples 510–511 cm, 450–451 cm and 300–301 cm from this interval share many characteristics, indicating only minor changes in organic matter source during this interval. The samples have relatively high contributions of vitrinites in group A and these are potentially derived from Cretaceous carbon bearing sediments (Dam et al., 1998; Dewing et al., 2007; Gentzis and Goodarzi, 1991; Mukhopadhyay et al., 1997). However, the larger contribution of the group B vitrinites in sample 300–301 cm indicates increased deposition derived from the Paleozoic sedimentary rocks (Harrison et al., 2008).

6.1.3. 130–4.5 cm

The upper ~130 cm of the core records the lowest average age offset of 2300 years, reflecting a further decreased influence of allochthonous organic matter. This is recorded by the highest $\delta^{13}C_{org}$ (−21.6‰) and HI (~95 mgHC g^{-1} TOC) together with low OI (~95 mgHC g^{-1} TOC), (Boucsein et al., 2002; Caron et al., 2019; Carrie et al., 2012; Fahl and Stein, 1999; Lafargue et al., 1998). The relatively high HI in this upper most part of the core could potentially be the result of lower organic matter degradation and therefore would not be an indication of increased marine productivity alone. Elevated HI values in the upper parts of sediments cores have been recorded in other studies and interpreted to result from lower degradation of fresh labile organic matter in the top samples (Bailey et al., 2013; Carrie et al., 2012; Disnar et al., 2003; Sanei et al., 2005; Wagner and Henrich, 1994).

The results of the organic petrography sample at 75–76 cm show that the majority of the vitrinites (64%) are thermally immature and thus placed in group A. However, the large group B (34%) suggests two main sources of sediment and organic matter, possibly from West Greenland and the Canadian Arctic Islands (Dam et al., 1998; Dewing et al., 2007; Gentzis and Goodarzi, 1991; Harrison et al., 2008). The petrographic results of this sample compared to sample depth 300–301 cm, 450–451 cm and 510–511 cm, do not exhibit major changes in the maceral composition indicative of minimal source area changes.

6.2. Cause of age offset

The age discrepancies that often occur between radiocarbon dates performed on bulk sediments and calcareous fossils have already been discussed extensively in previous studies. However, these studies primarily deal with lake sediments and only a few studies include marine sediment records. In the marine realm, studies have shown that elevated influence of reworked organic matter from terrigenous sources lead to erroneous bulk organic matter radiocarbon dates. Further, radiocarbon datings performed on shells appeared to be younger compared to radiocarbon datings of organic material (Andrews et al., 1985; Fillon et al., 1981; Giraudeau et al., 2020; Licht et al., 1998). To make up for these age discrepancies, various age correction methods have been applied on bulk organic material radiocarbon dates, including corrections using a constant correction factor (Andrews et al., 1985; Fillon et al., 1981; Giraudeau et al., 2020; Licht et al., 1998; Muschitiello et al., 2020). In estuarine and lake deposits, the age offsets are primarily caused by changes in sediment source and the influx of older reworked

^{14}C depleted organic matter (Grimm et al., 2009; Lougheed et al., 2017; Rößler et al., 2011; Strunk et al., 2020; Larsen et al., 2015). Overall, these studies suggest that the largest discrepancies between dates on fossils and on bulk sediment are found in intervals displaying changes in the environmental settings including lake stratification, changes in the "hard water effect", variations in sediment source material and transitions from a lacustrine to a marine environment.

In marine settings, radiocarbon dating is highly affected by the marine reservoir effect, which is not constant in marine environments that experience extensive oceanographic changes over time (e.g. Eiríksson et al., 2000, 2004). Changes in ocean circulation and carbon source pathways can affect the marine reservoir age. In our study, we applied a constant reservoir correction of $\Delta R = 140 \pm 30$ years in relation to the standard marine reservoir effect used in Marine13 (Reimer et al., 2013). However, the drastic change in the environment at ~614 cm might have been linked to a change in the oceanographic ventilation at that time (Hansen et al., 2020), which may have caused a change in marine reservoir age. Nevertheless, since we do not possess any data suggesting a more suitable marine reservoir age for the bottom most part of the core, the same constant reservoir age correction was applied for this lower section.

Our results show that changes in sedimentary carbon sources at our study site alter the age offsets between the bulk organic matter and microfossil dates. In intervals where HI values are high, indicating high concentration of contemporary autochthonous organic matter, the age offset between the bulk organic matter and the foraminiferal dates is comparatively low, while intervals with lower HI values and thus less influx of young carbon are characterized by a larger age difference. Hence, the high influx of contemporary marine algal produced organic matter shown by high HI may dilute the effect of the small presence of older ^{14}C-depleted organic matter observed in the organic petrography analysis. Additionally, our results indicate that high age offsets are measured in samples with relatively low TOC content. This has also been observed in studies of lake sediment cores from central North America and Greenland (Grimm et al., 2009; Strunk et al., 2020).

As mentioned in section 3.4, TOC is composed of both pyrolysable (S2 and S3) and residual fractions. In a marine system where the deposition of organic carbon is primarily supplied by contemporary marine algal produced organic matter, TOC is composed mainly of organic matter with high S2 content. If the depositional setting remains constant, the sediment record of such a system typically shows a strong linear correlation between S2 and TOC. This line intercepts at the origin indicating that at zero deposition of contemporary marine algal produced organic matter (represented by S2), there would be no TOC detected in the sediments. In reality, there is always a variable input of allochthonous organic carbon. These mostly land-derived organic carbon fractions do not contribute to the S2 content but still contain both S3 and residual organic carbon that can increase the TOC content of sediments. Therefore, the point where the S2:TOC linear regression line intercepts the TOC axis represents the amount of allochthonous organic carbon input in the marine system at the study site location (Cornford et al., 1998; Sanei et al., 2014). Consequently, the input of allochthonous organic carbon is controlled by changes in the sedimentation rates and environment.

Here, we apply the same concept using the regression line between S2 and TOC. The result shows that the S2:TOC plot (Fig. 6) represents the variation of marine algal productivity at our sediment core site and the degree to which it controls the TOC content of the sediments (614–4.5 cm). The S2:TOC graph shows two separate clusters, each representing distinct depositional environments represented by two segments of the sediment core (Fig. 6). The upper segment (4.5–614 cm core depth) shows a strong correlation ($R^2 = 0.88$) between the S2 and TOC. This upper segment represents the post-deglacial marine system. A strong linear relationship suggests here that the TOC content is dominantly controlled by algal input. The regression line intercepts the TOC axis at 0.6 wt%, indicating that the background allochthonous organic

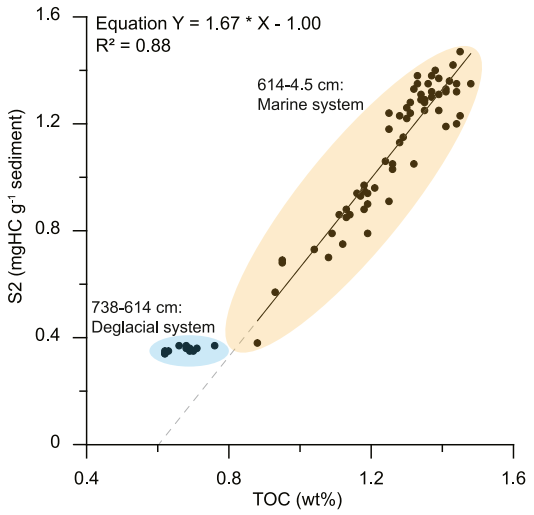

Fig. 6. The linear correlation between the S2 and TOC in the marine system shows that the regression line intercepts at 0.6 wt% TOC.

carbon in the sediments makes up 0.6 wt % of the TOC in the upper segment of the core (Cornford et al., 1998; Sanei et al., 2014).

In the lower portion of the core (614–738 cm core depth), TOC ranges from 0.6 to 0.8 wt% while S2 remains at a constant level of ~0.4 mgHC/g sediment. This segment covers the deglaciation period and thus a different depositional system.

Assuming that the concentration of allochthonous organic matter remains at an approximately constant level of 0.6 wt% throughout the sediment core, allows us to estimate the fraction of autochthonous organic carbon in the sediments:

$$\%\ authochthonous\ organic\ matter\ of\ TOC = \frac{TOCwt\% - 0.6wt\%}{TOCwt\%} * 100$$

This is a conservative, lower limit estimate of the allochthonous carbon content, as we know that this fraction of the organic carbon in the lower portion of the core can in fact fluctuate to up to 0.8 wt%.

The results show differences in the proportion of contemporary marine algal produced organic matter of the TOC in two segments of the core, i.e., 738-614 cm (stage 1) and 491-31 cm (stage 2). These two stages represent two depth intervals with distinctly different age offsets (Figs. 2 and 7), although stage 2 may be subdivided into two zones with somewhat different age offsets (Fig. 2). Based on these calculations, the autochthonous organic matter fraction of the TOC in stage 1 range from 3.2 to 31.8% (12.0% in average), demonstrating that, on average, around 88% of the TOC consists of allochthonous organic matter. This

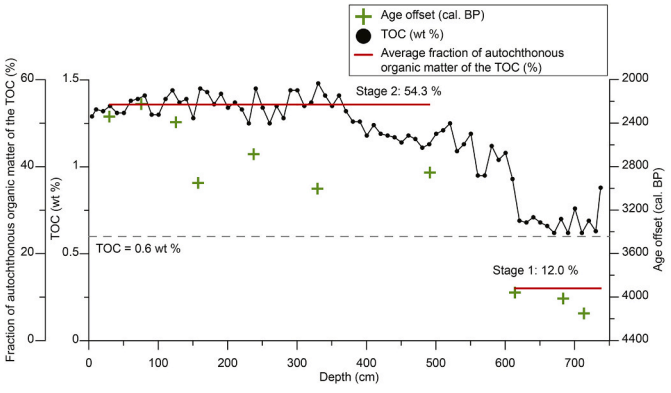

Fig. 7. TOC (wt%), age offset (cal. BP) and estimated average fraction of autochthonous marine algal produced organic matter of the TOC (%) for the two stages plotted against core depth.

high contribution of old organic matter fraction to the bulk TOC content clearly affects the record high age offsets of over 4000 years on average during this interval, with only minor variations (between 3960 and 4150 years).

Stage 2 is clearly different from stage 1 by having a much larger fraction of contemporary marine algal produced organic matter in the TOC with values, varying from 49.9% to 59.9% (average: 54.3%), indicating that the average proportion of allochthonous carbon is 45.7%. Here, the age offset varies between 2225 and 3000 years (average: 2640 years), with the lowest age offset in the top part. The age offset also fluctuates more than in the shorter stage 1. The lower age offset at the top of the core as well as the fluctuating offset in stage 1 may be ascribed to varying influx of allochthonous organic matter, with the largest amount of contemporary marine organic matter in the younger part of the core, where it has not yet been subjected to the same degree of degradation, that may occur deeper in the sediment.

Our estimated contribution of contemporary marine algal produced organic matter to the bulk TOC content, assumes a constant contribution of allochthonous organic carbon. In marine settings, however, this mostly terrigenous organic carbon fraction also fluctuates with changing source, as clearly shown by our organic petrology results (Fig. 5). This variation in the contribution of allochthonous organic matter could potentially explain some of the relatively higher age offsets in stage 2, where the TOC remains relatively high. It is possible that the proportions of the different carbon sources fluctuate in these depth intervals, due to short-term changes in depositional environment. Thus, the allochthonous organic matter contributions between 49.9% and 59.9% might explain the fluctuating age offsets in stage 2.

Based on our study, we do not recommend correcting bulk dates with a constant correction factor, as previously applied in other studies (Andrews et al., 1985; Licht et al., 1998; Giraudeau et al., 2020), due to changes in organic matter sources that appear to fluctuate vastly even on a local scale, as also proposed by Strunk et al. (2020). In future studies, a quantification of the organic components during the organic petrography analysis could provide valuable information in assessing the relative effect these components have on the age offsets compared to HI, OI, $\delta^{13}C_{org}$ and TOC.

7. Conclusion

We investigated the age offsets between radiocarbon dates obtained from mainly benthic foraminifera and bulk organic matter in a Holocene marine sediment core from the eastern Baffin Bay. Based on the results of the comparison of the age offset with X-ray fluorescence data, organic pyrolysis (TOC, HI, OI), $\delta^{13}C_{org}$ and organic petrography, the following conclusions can be made:

1. AMS ^{14}C dates based on bulk organic matter are on average 3000 years older than radiocarbon dates based on microfossils (mainly benthic and planktonic foraminifera) at our site. The age offset decreases towards the core top, possibly associated to a combination of increased production of contemporary marine algal produced organic matter and reduced advection of allochthonous (typically older) organic matter to the study site.
2. Increased age offsets correlate with reduced algal production of marine organic matter as indicated by low HI and $\delta^{13}C_{org}$ values and with higher values of the terrigenous indicators OI, Rb/Br and K.
3. Based on the results of the organic petrography analysis, three main sources of old terrigenous ^{14}C-depleted carbon were identified based on distinctions in thermal maturity; the A group with less mature vitrinites with mean %Ro of 0.7% possibly derived from Cretaceous outcrops from West Greenland or the Canadian Arctic Archipelago. The B group consists of vitrinites with mean %Ro of 1.6% potentially derived from outcrops of Paleozoic rocks from the Northeastern Canadian Arctic islands. Highly mature inertinites in the C group (mean %Ro of 2.5%) could be sourced from West Greenland Disko Bugt sediments that have been thermally altered by Paleogene volcanism. They could also be windblown charred wood from forest fires.
4. Down core changes in the relative distribution of the different organic macerals support the investigation of changes in sediment and organic matter sources, which might affect the age offset variations.
5. Quantification of down core changes in the amount of autochthonous organic material from marine algae compared to allochtonous organic material aids the understanding of changes in age offset: Higher percentages of autochthonous organic matter and lower percentages of older allochthonous organic matter in TOC will reduce the age offsets, and *vice versa*.

Data availability

Data is available at the PANGAEA database (https://doi.pangaea.de/10.1594/PANGAEA.928655), or by corresponding with Katrine Elnegaard Hansen (katrine.elnegaard@geo.au.dk) or Marit-Solveig Seidenkrantz (mss@geo.au.dk).

Author contribution

M-SS, CP, KEH and HS developed the research idea. GM led the research cruise and collected marine sediment core AMD14-204C. Organic pyrolysis and organic petrography were conducted by KEH, AR and HS. LW carried out the foraminiferal-based radiocarbon datings. JG provided four foraminiferal and ten bulk organic matter radiocarbon datings together with the XRF record. KEH prepared the manuscript with contributions from all co-authors.

Declaration of competing interest

The authors declare that they have no known competing financial interests or personal relationships that could have appeared to influence the work reported in this paper.

Acknowledgements

We wish to thank the captain, crew and the scientific party of the CCGS *Amundsen* 2014 expedition for their work in retrieval of the marine sediment core AMD14-204C, financially supported by the Fondation Total, the French Agence Nationale de la Recherche (GreenEdge project), the Network of Centres of Excellence ArcticNet, and the ERC STG ICEPROXY 203441. Additionally, we wish to thank Eleanor Georgiadis, Philippe Martinez, and Isabelle Billy for running the X-ray fluorescence spectroscopy of the core at the EPOC laboratory at the University of Bordeaux, and for composing these data sets. We would also like to thank Rikke Brok Jensen, Aarhus University, for preparing the sediment samples for organic petrography analysis. We are also grateful to Thomas Ulrich, Aarhus University, who demonstrated how to polish samples for organic petrography. Finally we thank an unnamed reviewer for their valuable comments and suggestions.

Appendix A. Supplementary data

Supplementary data to this article can be found online at https://doi.org/10.1016/j.quageo.2021.101242.

Financial support

This research has been supported by the Danish Council for Independent Research (grant no. 7014- 00113B/FNU) to Marit-Solveig Seidenkrantz (G-Ice project).

References

Abdelmalak, M.M., Polteau, S., 2020. The thermal maturity of sedimentary basins as revealed by magnetic mineralogy. Basin Res. 1–21. https://doi.org/10.1111/bre.12439.

Andrews, J.T., Jull, A.J.T., Donahue, D.J., Short, S.K., Osterman, L.E., 1985. Sedimentation rates in Baffin Island fiord cores from comparative radiocarbon dates (Canada). Can. J. Earth Sci. 22 (12), 1827–1834. https://doi.org/10.1139/e85-194.

Arthur, M.A., Anderson, T.F., Kaplan, I.R., Veizer, J., Land, L.S., 1983. Stable Isotopes in Sedimentary Geology. https://doi.org/10.2110/scn.83.10.

Bailey, J.N.L., Macdonald, R.W., Sanei, H., Outridge, P.M., Johannessen, S.C., Hochheim, K., Barber, D., Stern, G.A., 2013. Change at the margin of the North Water Polynya, Baffin Bay, inferred from organic matter records in dated sediment cores. Mar. Geol. 341, 1–13. https://doi.org/10.1016/j.margeo.2013.04.017.

https://www.radiocarbon.com/pretreatment-carbon-dating.htm, 2000–. (Accessed 12 May 2020).

Boucsein, B., Stein, R., 2000. Particulate organic matter in surface sediments of the Laptev Sea (Arctic Ocean): application of maceral analysis as organic-carbon-source indicator. Mar. Geol. 162 (2–4), 573–586. https://doi.org/10.1016/S0025-3227(99)00066-3.

Boucsein, B., Knies, J., Stein, R., 2002. Organic matter deposition along the Kara and Laptev Seas continental margin (eastern Arctic Ocean) during last deglaciation and Holocene: evidence from organic-geochemical and petrographical data. Mar. Geol. 183 (1–4), 67–87. https://doi.org/10.1016/S0025-3227(01)00249-3.

Bustin, R.M., Barnes, M.A., Barnes, W.C., 1985. Diagenesis 10. Quantification and Modelling of Organic diagenesis., Geosci. Canada.

Caron, M., Rochon, A., Carlos, J., Serrano, M., Onge, G.S.T., 2019. Evolution of sea-surface conditions on the northwestern Greenland margin during the Holocene. J. Quat. Sci. 1–12. https://doi.org/10.1002/jqs.3146.

Carrie, J., Sanei, H., Stern, G., 2012. Standardisation of Rock-Eval pyrolysis for the analysis of recent sediments and soils. Org. Geochem. 46, 38–53. https://doi.org/10.1016/j.orggeochem.2012.01.011.

Cornford, C., Gardner, P., Burgess, C., 1998. Geochemical truths in large data sets. I: geochemical screening data. Org. Geochem. 29, 519–530. https://doi.org/10.1016/S0146-6380(98)00189-2.

Dam, G., Nøhr-Hansen, H., Christiansen, F.G., Bojesen-Koefoed, J.A., Laier, T., 1998. The oldest marine cretaceous sediments in west Greenland (Umiivik-1 borehole) – record of the cenomanian–turonian anoxic event? GEUS Bull. 180, 128–137. https://doi.org/10.34194/ggub.v180.5096.

Descolas-Gros, C., Fontugne, M.R., 1985. Carbon fixation in marine phytoplankton: carboxylase activities and stable carbon-isotope ratios; physiological and paleoclimatological aspects. Mar. Biol. 87 (1), 1–6. https://doi.org/10.1007/BF00396999.

Dewing, K., Obermajer, M., Goodarzi, F., 2007. Geological and Geochemical Data from the Canadian Arctic Islands. Part III: Organic Matter Reflectance Data.

Disnar, J.R., Guillet, B., Keravis, D., Di-Giovanni, C., Sebag, D., 2003. Soil organic matter (SOM) characterization by Rock-Eval pyrolysis: scope and limitations. Org. Geochem. https://doi.org/10.1016/S0146-6380(02)00239-5.

Drinkwater, K.F., 1996. Atmospheric and oceanic variability in the northwest Atlantic during the 1980s and early 1990s. J. Northwest Atl. Fish. Sci. 18, 77–97. https://doi.org/10.2960/J.v18.a6.

Ehleringer R., James, Cerling E., Thure, Helliker R., Brent, 1997. C4 photosynthesis, atmospheric CO2, and climate. Oecologia 112, 285–299. https://doi.org/10.1007/s004420050311.

Eiríksson, J., Knudsen, K.L., Haflidason, H., Heinemeier, J., 2000. Chronology of late Holocene climatic events in the northern North Atlantic based on AMS 14C dates and tephra markers from the volcano Hekla, Iceland. J. Quat. Sci. 15 (6), 573–580. https://doi.org/10.1002/1099-1417(200009)15:6<573::AID-JQS554>3.0.CO;2-A.

Eiríksson, J., Larsen, G., Knudsen, K.L., Heinemeier, J., Símonarson, L.A., 2004. Marine reservoir age variability and water mass distribution in the Iceland Sea. In: Quaternary Science Reviews.

Escher, J., Pulvertaft, T., 1995. Geological map of Greenland. In: Geological Survey of Greenland, vol. 1, 2500000. Copenhagen.

Fahl, K., Stein, R., 1997. Modern organic carbon deposition in the Laptev Sea and the adjacent continental slope: surface water productivity vs. terrigenous input. Org. Geochem. 26 (5–6), 379–390. https://doi.org/10.1016/S0146-6380(97)00007-7.

Fahl, K., Stein, R., 1999. Biomarkers as organic-carbon-source and environmental indicators in the late quaternary Arctic Ocean: problems and perspectives. Mar. Chem. 63 (3–4), 293–309. https://doi.org/10.1016/S0304-4203(98)00068-1.

Fillon, R.H., Hardy, I.W., Wagner, F.J.E., Andrews, J.T., Josenhans, H., 1981. Labrador Shelf: shell and total organic matter 14C date discrepancies. Curr. Res. part B. Geol. Surv. Canada 105–111. Paper 81-1.

Gentzis, T., Goodarzi, F., 1991. Thermal maturity and hydrocarbon potential of the sedimentary succession from the Hecla field in Sverdrup Basin, Arctic Canada. Int. J. Coal Geol. 19, 483–517. https://doi.org/10.1016/0166-5162(91)90031-D.

Giraudeau, J., Georgiadis, E., Caron, M., Martinez, P., Saint-Onge, G., Billy, I., Lebleu, P., Ther, O., Massé, G., 2020. A high-resolution elemental record of post-glacial lithic sedimentation in Upernavik Trough, western Greenland: history of ice-sheet dynamics and ocean circulation changes over the last 9100 years. Global Planet. Change 191 (103217), 10.1016/j.gloplacha.2020.103217.

Green, P.F., 2003. Thermal History Reconstruction in the Ataa-1, Gane-1, Gant-1, Gro-3 and Umiivik-1 Boreholes, Onshore West Greenland, Based on Afta®, Vitrinite Reflectance and Apatite (U-Th)/He Dating. A Report Prepared for GEUS by Geotrack International Pty Ltd, Geotrack Rep, vol. 883, pp. 1–205 [online] Available from: http://www.geolsoc.org.uk/webdav/site/GSL/shared/Sup_pubs/2005/SUP18212Report.pdf.

Gregersen, U., Knutz, P.C., Nøhr-Hansen, H., Sheldon, E., Hopper, J.R., 2020. Tectonostratigraphy and evolution of the West Greenland continental margin. Bull. Geol. Soc. Den. 67, 1–21. https://doi.org/10.37570/bgsd-2019-67-01.

Grimm, E.C., Maher, L.J., Nelson, D.M., 2009. The magnitude of error in conventional bulk-sediment radiocarbon dates from central North America. Quat. Res. 72 (2), 301–308. https://doi.org/10.1016/j.yqres.2009.05.006.

Hansen, K.E., Giraudeau, J., Wacker, L., Pearce, C., Seidenkrantz, M.-S., 2020. Reconstruction of Holocene oceanographic conditions in the northeastern Baffin Bay. Clim. Past Discuss. https://doi.org/10.5194/cp-2019-152 [online] Available from: n.d).

Harrison, J.C., Nowlan, G.S., Lehnert, O., 2008. Thermal maturity of cambrian to devonian rocks of northeastern Ellesmere island. Geol. Surv. Can. Bull. 592, 169–185.

Harrison, J.C., St-Onge, M.R., Petrov, O.V., Strelnikov, S.I., Lopatin, B.G., Wilson, F.H., Tella, S., Paul, D., Lynds, T., Shokalsky, S.P., Hults, C.K., Bergman, S., Jepsen, H.F., Solli, A., 2011. Geological Map of the Arctic.

Haubner, K., Box, J.E., Schlegel, N.J., Larour, E.Y., Morlighem, M., Solgaard, A.M., Kjeldsen, K.K., Larsen, S.H., Rignot, E., Dupont, T.K., Kjær, K.H., 2018. Simulating ice thickness and velocity evolution of Upernavik Isstrøm 1849–2012 by forcing prescribed terminus positions in ISSM. Cryosph 12 (4), 1511–1522. https://doi.org/10.5194/tc-12-1511-2018.

Jackson, R., Carlson, A.E., Hillaire-Marcel, C., Wacker, L., Vogt, C., Kucera, M., 2017. Asynchronous instability of the North American-Arctic and Greenland ice sheets during the last deglaciation. Quat. Sci. Rev. 164, 140–153. https://doi.org/10.1016/j.quascirev.2017.03.020.

Jansen, J.H.F., Van Der Gaast, S.J., Koster, B., Vaars, A.J., 1998. CORTEX, a shipboard XRF-scanner for element analyses in split sediment cores. Mar. Geol. 151 (1–4), 143–153. https://doi.org/10.1016/S0025-3227(98)00074-7.

Japsen, P., Green, P.F., Chalmers, J.A., 2005. Separation of palaeogene and Neogene uplift on Nuussuaq, west Greenland. J. Geol. Soc. London. 162 (2), 299–314. https://doi.org/10.1144/0016-764904-038.

van Krevelen, D.W., 1993. Coal: Typology - Chemistry - Physics - Constitution, third ed. Elsevier Science, Amsterdam.

Lafargue, E., Marquis, F., Pillot, D., 1998. Rock-eval 6 applications in hydrocarbon exploration, production, and soil contamination studies, rev. l'Institut Français du Pétrole 53, 421–437. https://doi.org/10.2516/ogst:1998036.

Larsen, N.K., Kjær, K.H., Lecavalier, B., Bjørk, A.A., Colding, S., Huybrechts, P., Jakobsen, K.E., Kjeldsen, K.K., Knudsen, K.L., Odgaard, B.V., Olsen, J., 2015. The response of the southern Greenland ice sheet to the Holocene thermal maximum. Geology 43 (4), 291–294. https://doi.org/10.1130/G36476.1.

Law, C.A., 1999. Evaluating source rocks. In: Beaumont, E.A., foster (Eds.), Exploring for Oil and Gas Traps. AAPG., pp. 6–41

Licht, K.J., Cunningham, W.L., Andrews, J.T., Domack, E.W., Jennings, A.E., 1998. Establishing chronologies from acid-insoluble organic 14C dates on antarctic (Ross sea) and arctic (north atlantic) marine sediments, 17 (2), 203–216. https://doi.org/10.3402/polar.v17i2.6619.

Liu, B., Teng, J., Mastalerz, M., Schieber, J., 2020. Assessing the thermal maturity of black shales using vitrinite reflectance: insights from Devonian black shales in the eastern United States. Int. J. Coal Geol. 220 (February), 103426. https://doi.org/10.1016/j.coal.2020.103426.

Lloyd, J., Moros, M., Perner, K., Telford, R.J., Kuijpers, A., Jansen, E., McCarthy, D., 2011. A 100 yr record of ocean temperature control on the stability of Jakobshavn Isbrae, West Greenland. Geology 39 (9), 867–870. https://doi.org/10.1130/G32076.1.

Lougheed, B.C., Obrochta, S.P., Lenz, C., Mellström, A., Metcalfe, B., Muscheler, R., Reinholdsson, M., Snowball, I., Zillén, L., 2017. Bulk sediment 14C dating in an estuarine environment: how accurate can it be? Paleoceanography 32 (2), 123–131. https://doi.org/10.1002/2016PA002960.

Meyers, P.A., 1994. Preservation of elemental and isotopic source identification of sedimentary organic matter. Chem. Geol. 114 (3–4), 289–302. https://doi.org/10.1016/0009-2541(94)90059-0.

Morlighem, M., Williams, C.N., Rignot, E., An, L., Arndt, J.E., Bamber, J.L., Catania, G., Chauché, N., Dowdeswell, J.A., Dorschel, B., Fenty, I., Hogan, K., Howat, I., Hubbard, A., Jakobsson, M., Jordan, T.M., Kjeldsen, K.K., Millan, R., Mayer, L., Mouginot, J., Noël, B.P.Y., O'Cofaigh, C., Palmer, S., Rysgaard, S., Seroussi, H., Siegert, M.J., Slabon, P., Straneo, F., van den Broeke, M.R., Weinrebe, W., Wood, M., Zinglersen, K.B., 2017. BedMachine v3: complete bed topography and ocean bathymetry mapping of Greenland from multibeam echo sounding combined with mass conservation. Geophys. Res. Lett. https://doi.org/10.1002/2017GL074954.

Mukhopadhyay, P.K., Goodarzi, F., Kruge, M.A., Alimi, M.H., 1997. Comparison of source rock geochemistry of selected rocks from the Schei Point group and Ringnes formation, Sverdrup basin, arctic Canada. Int. J. Coal Geol. 34, 225–260. https://doi.org/10.1016/S0166-5162(97)00024-4.

Münchow, A., Falkner, K.K., Melling, H., 2015. Baffin island and west Greenland current systems in northern Baffin Bay. Prog. Oceanogr. 132, 305–317. https://doi.org/10.1016/j.pocean.2014.04.001.

Muschitiello, F., O'Regan, M., Martens, J., West, G., Gustafsson, Ö., Jakobsson, M., 2020. A new 30 000-year chronology for rapidly deposited sediments on the Lomonosov Ridge using bulk radiocarbon dating and probabilistic stratigraphic alignment. Geochronology 2 (1), 81–91. https://doi.org/10.5194/gchron-2-81-2020.

Nagler, T., Rott, H., Hetzenecker, M., Wuite, J., Potin, P., 2015. The Sentinel-1 mission: new opportunities for ice sheet observations. Rem. Sens. https://doi.org/10.3390/rs70709371.

Outridge, P.M., Sanei, H., Stern, G.A., Hamilton, P.B., Goodarzi, F., 2007. Evidence for control of mercury accumulation rates in Canadian High Arctic Lake sediments by

variations of aquatic primary productivity. Environ. Sci. Technol. 41 (15), 5259–5265. https://doi.org/10.1021/es070408x.
Perner, K., Moros, M., Jennings, A., Lloyd, J.M., Knudsen, K.L., 2012. Holocene palaeoceanographic evolution off West Greenland. Holocene 23 (3), 374–387. https://doi.org/10.1177/0959683612460785.
Pruysers, P.A., de Lange, G.J., Middelburg, J.J., 1991. Geochemistry of eastern Mediterranean sediments: primary sediment composition and diagenetic alterations. Mar. Geol. 100 (1–4), 137–154. https://doi.org/10.1016/0025-3227(91)90230-2.
Ramsey, C.B., 2008. Deposition models for chronological records. Quat. Sci. Rev. 27 (1–2), 42–60. https://doi.org/10.1016/j.quascirev.2007.01.019.
Reimer, P.J., Bard, E., Bayliss, A., Beck, J.W., Blackwell, P.G., Ramsey, C.B., Buck, C.E., Cheng, H., Edwards, R.L., Friedrich, M., Grootes, P.M., Guilderson, T.P., Haflidason, H., Hajdas, I., Hatté, C., Heaton, T.J., Hoffmann, D.L., Hogg, A.G., Hughen, K.A., Kaiser, K.F., Kromer, B., Manning, S.W., Niu, M., Reimer, R.W., Richards, D.A., Scott, E.M., Southon, J.R., Staff, R.A., Turney, C.S.M., van der Plicht, J., 2013. IntCal13 and Marine13 radiocarbon age calibration curves 0–50,000 Years cal BP. Radiocarbon 55 (4), 1869–1887. https://doi.org/10.2458/azu_js_rc.55.16947.
Ren, J., Jiang, H., Seidenkrantz, M.S., Kuijpers, A., 2009. A diatom-based reconstruction of Early Holocene hydrographic and climatic change in a southwest Greenland fjord. Mar. Micropaleontol. 70 (3–4), 166–176. https://doi.org/10.1016/j.marmicro.2008.12.003.
Rößler, D., Moros, M., Lemke, W., 2011. The Littorina transgression in the southwestern Baltic Sea: new insights based on proxy methods and radiocarbon dating of sediment cores. Boreas 40 (2), 231–241. https://doi.org/10.1111/j.1502-3885.2010.00180.x.
Saito, S., 1998. Major and trace element geochemistry of sediments from East Greenland Continental Rise: an implication for sediment provenance and source area weathering. In: Saunders, A.D., Larsen, H.C., Wise, S.W. (Eds.), Proceedings of the Ocean Drilling Program, 152 Scientific Results, vol. 152. Ocean Drilling Program, College Station, TX, pp. 19–28.
Sanei, H., Goodarzi, F., 2006. Relationship between organic matter and mercury in recent lake sediment: the physical-geochemical aspects, Appl. Geochemistry 21 (11), 1900–1912. https://doi.org/10.1016/j.apgeochem.2006.08.015.
Sanei, H., Goodarzi, F., Snowdon, L.R., Stasiuk, L.D., Van Der Flier-Keller, E., 2000. Characterizing the recent sediments from pigeon lake, alberta as related to anthropogenic and natural fluxes. Environ. Geosci. 7 (4), 177–189. https://doi.org/10.1046/j.1526-0984.2000.74007.x.
Sanei, H., Goodarzi, F., Van der Flier-Keller, E., 2001. Historical variation of elements with respect to different geochemical fractions in recent sediments from Pigeon Lake, Alberta, Canada. J. Environ. Monit. 3, 27–36. https://doi.org/10.1039/b006819p.
Sanei, H., Stasiuk, L.D., Goodarzi, F., 2005. Petrological changes occurring in organic matter from Recent lacustrine sediments during thermal alteration by Rock-Eval pyrolysis. Org. Geochem. https://doi.org/10.1016/j.orggeochem.2005.02.009.
Sanei, H., Petersen, H.I., Schovsbo, N.H., Jiang, C., Goodsite, M.E., 2014. Petrographic and geochemical composition of kerogen in the Furongian (U. Cambrian) Alum Shale, central Sweden: reflections on the petroleum generation potential. Int. J. Coal Geol. 132, 158–169. https://doi.org/10.1016/j.coal.2014.08.010.
Scott, A.C., Glasspool, I.J., 2007. Observations and experiments on the origin and formation of inertinite group macerals. Int. J. Coal Geol. 70 (1–3 SPEC. ISS.), 53–66. https://doi.org/10.1016/j.coal.2006.02.009.
Seidenkrantz, M.S., Aagaard-Sørensen, S., Sulsbrück, H., Kuijpers, A., Jensen, K.G., Kunzendorf, H., 2007. Hydrography and climate of the last 4400 years in a SW Greenland fjord: implications for Labrador Sea palaeoceanography. Holocene 17 (3), 387–401. https://doi.org/10.1177/0959683607075840.
Stach, E., Murchison, D., Mackowsky, M.T., Teichmüller, M., 1982. Stach's textbook of coal petrology. In: Stach, E., Murchison, D.G., Borntraeger (Eds.), third ed. University of California.
Steenfelt, A., 2001. Geochemical Atlas of Greenland – West and South Greenland.
Steenfelt, A., Thomassen, B., Lind, M., Kyed, J., 1998. Karrat 97: reconnaissance mineral exploration in central 761 West Greenland. Geol. Greenl. Surv. Bull. 180, 73–80.
Strunk, A., Olsen, J., Sanei, H., Rudra, A., Larsen, N.K., 2020. Improving the reliability of bulk sediment radiocarbon dating. Quat. Sci. Rev. 15 (106442) https://doi.org/10.1016/j.quascirev.2020.106442.
Tang, C.C.L., Ross, C.K., Yao, T., Petrie, B., DeTracey, B.M., Dunlap, E., 2004. The circulation, water masses and sea-ice of Baffin Bay. Prog. Oceanogr. 63 (4), 183–228. https://doi.org/10.1016/j.pocean.2004.09.005.
Vermassen, F., Andreasen, N., Wangner, D.J., Thibault, N., Seidenkrantz, M.S., Jackson, R., Schmidt, S., Kjær, K.H., Andresen, C.S., 2019a. A reconstruction of warm-water inflow to Upernavik Isstrøm since 1925 CE and its relation to glacier retreat. Clim. Past 15 (3), 1171–1186. https://doi.org/10.5194/cp-15-1171-2019.
Vermassen, F., Wangner, D.J., Dyke, L.M., Schmidt, S., Cordua, A.E., Kjær, K.H., Haubner, K., Andresen, C.S., 2019b. Evaluating ice-rafted debris as a proxy for glacier calving in Upernavik Isfjord, NW Greenland. J. Quat. Sci. 34 (3), 258–267. https://doi.org/10.1002/jqs.3095.
Wagner, T., Henrich, R., 1994. Organo- and lithofacies of glacial-interglacial deposits in the Norwegian-Greenland Sea: responses to paleoceanographic and paleoclimatic changes. Mar. Geol. 120, 335–364.
Weatherall, P., Marks, K.M., Jakobsson, M., Schmitt, T., Tani, S., Arndt, J.E., Rovere, M., Chayes, D., Ferrini, V., Wigley, R., 2015. A new digital bathymetric model of the world's oceans. Earth Sp. Sci. https://doi.org/10.1002/2015EA000107.